



Kent Academic Repository

Mulligan, Christopher, Fitzgerald, Gabriel A, Wang, Da-Neng and Mindell, Joseph A (2014) *Functional characterization of a Na⁺-dependent dicarboxylate transporter from Vibrio cholerae*. *The Journal of General Physiology*, 143 (6). pp. 745-759. ISSN 0022-1295.

Downloaded from

<https://kar.kent.ac.uk/61672/> The University of Kent's Academic Repository KAR

The version of record is available from

<https://doi.org/10.1085/jgp.201311141>

This document version

Author's Accepted Manuscript

DOI for this version

Licence for this version

UNSPECIFIED

Additional information

Versions of research works

Versions of Record

If this version is the version of record, it is the same as the published version available on the publisher's web site. Cite as the published version.

Author Accepted Manuscripts

If this document is identified as the Author Accepted Manuscript it is the version after peer review but before type setting, copy editing or publisher branding. Cite as Surname, Initial. (Year) 'Title of article'. To be published in **Title of Journal**, Volume and issue numbers [peer-reviewed accepted version]. Available at: DOI or URL (Accessed: date).

Enquiries

If you have questions about this document contact ResearchSupport@kent.ac.uk. Please include the URL of the record in KAR. If you believe that your, or a third party's rights have been compromised through this document please see our [Take Down policy](https://www.kent.ac.uk/guides/kar-the-kent-academic-repository#policies) (available from <https://www.kent.ac.uk/guides/kar-the-kent-academic-repository#policies>).

Functional characterization of a Na⁺-dependent dicarboxylate transporter from *Vibrio cholerae*

Christopher Mulligan¹, Gabriel A. Fitzgerald¹, Da-Neng Wang^{2,3} and Joseph A. Mindell¹

¹Membrane Transport Biophysics Section, Porter Neuroscience Research Center, National Institute of Neurological Disorders and Stroke, National Institutes of Health, Bethesda, MD 20892.

²The Helen L. and Martin Kimmel Center for Biology and Medicine, Skirball Institute of Biomolecular Medicine.

³Department of Cell Biology, New York University School of Medicine, New York, NY 10016.

Running title: Functional characterization of VcINDY

To whom correspondence should be addressed: Joseph A. Mindell, Membrane Transport Biophysics Section, Porter Neuroscience Research Center, National Institute of Neurological Disorders and Stroke, National Institutes of Health, Bethesda, MD 20892, USA. Tel.: (301) 402-3473; Fax: (301) 435-5666; e-mail: mindellj@ninds.nih.gov.

Abstract

The SLC13 transporter family, whose members play key physiological roles in the regulation of fatty acid synthesis, adiposity, insulin resistance, and other processes, catalyze the transport of Krebs cycle intermediates and sulfate across the plasma membrane of mammalian cells. SLC13 transporters are part of the divalent anion:Na⁺ symporter (DASS) family which includes several well characterized bacterial members. Despite sharing significant sequence similarity, the functional characteristics of DASS family members differ with regard to their substrate and coupling ion dependence. The publication of a high resolution structure of VcINDY, a bacterial DASS family member, provides crucial structural insight into this transporter family. However, marrying this structural insight to the current functional understanding of this family also demands a comprehensive analysis of the transporter's functional properties. To this end, we purified VcINDY, reconstituted it into liposomes, and determined its basic functional characteristics. Our data demonstrate that VcINDY is a high affinity, Na⁺-dependent transporter with a preference for C₄⁻ and C₅-dicarboxylates. Transport of the model substrate, succinate, is highly pH dependent, consistent with VcINDY strongly preferring the substrate's dianionic form. VcINDY transport is electrogenic with succinate coupled to the transport of 3 or more Na⁺ ions. In contrast to succinate, citrate, bound in the VcINDY crystal structure (in an inward-facing conformation), seems to interact only weakly with the transporter *in vitro*. These transport properties together provide a functional framework for future experimental and computational examinations of the VcINDY transport mechanism.

Key words: Functional reconstitution, Membrane transport, Succinate, Transporters, Citrate

Introduction

In humans, members of the SLC13 transporter family catalyze the transport of di- and tricarboxylic acids, as well as sulfate, across the plasma membrane fulfilling a number physiological and pathophysiological roles (Bergeron et al., 2013). Citrate plays a major role in determining the metabolic status of the cell by acting as a key precursor and allosteric regulator of fatty acid synthesis (Spencer and Lowenstein, 1962), and by down-regulating both fatty acid β -oxidation and glycolysis (Garland et al., 1963; Denton and Randle, 1966; Ruderman et al., 1999). NaDC1 (SLC13A2) is found on the apical membranes of renal proximal tubule and appears to be important for the regulation of urinary citrate and the prevention of kidney stones (Ho et al., 2007), whereas its high affinity homolog, NaDC3 (SLC13A3) has a wide tissue distribution (Pajor, 2013). NaCT (SLC13A5) is responsible, in part, for the uptake of citrate into the cytosol of liver cells (Inoue et al., 2002b; Inoue et al., 2002c). Remarkably, deletion of NaCT in mice leads to protection against adiposity and insulin resistance, highlighting the integral role of these transporters to normal metabolic function and hinting at therapeutic potential in combating metabolic disease, obesity and diabetes (Birkenfeld et al., 2011). Members of the SLC13 family are approximately 50% identical to each other and display distinct functional properties. NaCT is primarily a citrate transporter, but can also transport C_4 -dicarboxylates, such as succinate, fumarate and malate (Inoue et al., 2002b). NaDC1 and NaDC3 are C_4 -dicarboxylate transporters with a low and high affinity, respectively, but also retain the ability to transport citrate (Pajor, 1995; Pajor and Sun, 1996; Kekuda et al., 1999; Pajor and Sun, 2000; Oshiro and Pajor, 2005). Two other SLC13 members (NaS1 (SLC13A1) and NaS2 (SLC13A4)) transport, among other compounds, divalent anions sulfate and selenate (Busch et al., 1994; Markovich et al., 2005). Despite differences in substrate affinity and specificity, all five SLC13 members couple the electrogenic transport of their respective substrates to the transport of multiple Na^+ ions.

The SLC13 transporters belong to a larger group of related transporters called the divalent anion:Na⁺ symporter (DASS) family (TCDB # 2.A.47) (Saier et al., 2006). Knockdown of a gene encoding a DASS family member (INDY, *I'm not dead yet*) in the fruit fly *Drosophila melanogaster* results in reduced fat storage and, interestingly, an extended lifespan phenotype, mimicking the effects of caloric restriction (Rogina et al., 2000). In contrast to its human counterparts, citrate and C₄-dicarboxylate transport by the fly homolog, DrINDY, is apparently electroneutral and cation-independent (Knauf et al., 2002). A number of bacterial DASS family members (~30% identical to human SLC13 family members) have also been studied, revealing functional characteristics sometimes similar but sometimes divergent compared with the human homologs. However the similarities are sufficient to suggest a similar architecture and shared basic mode of action (Hall and Pajor, 2007; Youn et al., 2008; Strickler et al., 2009; Pajor et al., 2013).

Recently, our understanding of the transport mechanism of this family took a significant forward step with the publication of a high resolution x-ray crystal structure of VcINDY, a SLC13 homolog from *Vibrio cholerae* (Mancusso et al., 2012) (Fig. 1A and B). VcINDY is 26-33% identical to SLC13 family members in amino acid sequence and, like other DASS family members, couples a Na⁺ gradient to the transport of succinate, a C₄-dicarboxylate, in cell-based assays (Mancusso et al., 2012). In these assays, transport of succinate is inhibited by the presence of other C₄-dicarboxylates; malate and fumarate, suggesting that they may also serve as substrates. On the other hand, citrate and glutamate only mildly inhibit succinate transport, whereas sulfate has no effect (Mancusso et al., 2012). Succinate, malate and citrate also confer thermostability to the detergent solubilized VcINDY protein (Mancusso et al., 2012), suggesting all three compounds interact with the protein. The 3.2 Å resolution crystal structure of VcINDY reveals a homodimeric protein with each protomer containing 11 transmembrane helices and 2 re-entrant hairpin loops; HP_{IN} and HP_{OUT} (Fig. 1A and B). In each protomer, conserved residues at the tips of HP_{IN} and HP_{OUT} coordinate the bound substrate, likely a single citrate molecule, and a single Na⁺ ion. A second predicted Na⁺ binding site lies at the tip of HP_{OUT}, but no Na⁺ ion is

detected at this location and the role of this putative binding site in Na⁺ binding and transport has not been functionally verified (Mancusso et al., 2012). Topological studies of VcINDY homologs and the location of the substrates in the crystal structure suggest that this structure of VcINDY represents the inward-facing state of the protein (Mancusso et al., 2012) (Fig. 1A). The bound citrate molecule has been proposed to be acting as a state-dependent inhibitor, trapping the protein in this inward-facing conformation, although there is little evidence to support this assertion. The structure and cell-based functional characterization of VcINDY clearly place it as a functional representative of the DASS family but leave key mechanistic questions unanswered, including its transport stoichiometry, the extent of its substrate selectivity, and its ion coupling.

Here, we address these functional questions for VcINDY by assaying the purified protein reconstituted into liposomes. Measuring transport activity using proteoliposomes has a number of advantages over using whole cells or membrane vesicles. In proteoliposomes the protein of interest can be reconstituted in isolation, eliminating the possibility of artifacts due to native transport activity in the bacterial cell or due to interactions with endogenous bacterial proteins (Chen and Wilson, 1986; Quick et al., 2006; Hall and Pajor, 2007). In addition, unlike cells, the reconstituted system provides complete control of both external and internal solutions and substrate catabolism is not a problem. Together, these features make the purified, reconstituted system an ideal setting for precise functional characterization of bacterial transporter proteins. Using this experimental approach, we demonstrate that VcINDY is a Na⁺ gradient-dependent, electrogenic, pH gradient-independent, C₄-dicarboxylate transporter with characteristics most similar to its mammalian homolog, NaDC3, the high affinity dicarboxylate transporter. These results are essential for further analysis of the transporter's mechanism and for initiating computational studies of VcINDY.

Materials and methods

Expression and purification

VcINDY was expressed and purified essentially as described previously (Mancusso et al., 2012). BL21-AI (Life Technologies) was transformed with pEThisINDY (a modified pET vector (Love et al., 2010) harboring the gene encoding VcINDY with a N-terminal deca-histidine tag) and grown in LB supplemented with 100 µg/ml kanamycin to A_{600} of 0.6, at which point, expression was induced by addition of 0.1 M IPTG and 6.6 mM (0.1% (w/v)) L-arabinose. Cultures were incubated overnight at 19°C then harvested and lysed using an EmulsiFlex-C3 homogenizer (Avestin) and the membrane fraction was isolated by ultracentrifugation. This membrane fraction was resuspended in buffer containing 50 mM Tris HCl, pH 8, 100 mM NaCl and 5% (v/v) glycerol. Protein was extracted from the membranes by addition of *n*-dodecyl-β-D-maltoside (DDM, Anatrace) to a final concentration of 20 mM. Insoluble material was removed by ultracentrifugation and the detergent-solubilized fraction was incubated with Talon metal affinity resin (Clontech) overnight at 4°C. The resin was washed; first with 20 columns volumes (CV) of the above buffer supplemented with 2 mM DDM and 10 mM imidazole and then with 20 CV of the same buffer supplemented with 2 mM DDM and 20 mM imidazole. Bound protein was eluted by addition of buffer containing 300 mM imidazole. The histidine tag was removed by incubation with his-tagged TEV protease overnight at 4°C. The TEV protease and uncleaved protein were removed by reapplying the sample to Talon resin. The protein not sequestered by the resin was collected, concentrated and exchanged into buffer containing 50 mM Tris/HEPES, pH 7.5, 150 mM NaCl, 5% glycerol, 3 mM decyl-β-D-maltoside (DM, Anatrace). The protein was either used immediately or snap-frozen and stored at -80°C.

Protein reconstitution

Protein was functionally reconstituted into liposomes essentially as described previously for the aspartate transporter Glt_{ph} (Ryan et al., 2009). Lipids, in a ratio of 3:1 *E. coli* polar lipids to POPC (Avanti

Polar Lipids), were dried and resuspended to a concentration of 10 mg/ml in internal solution (the nature of the internal solution was dependent on the nature of the transport assay, typically it was 20 mM Tris/HEPES, pH 7.5, 1 mM NaCl and 199 mM KCl). Following 5 freeze-thaw cycles, the lipids were extruded through 400 nm filter and titrated with Triton X-100. The incorporation of Triton X-100 was monitored using the A_{540} reading and additions were stopped after reaching the saturation point. Protein was added to the lipids in a ratio of 1.5 μg protein/mg lipid. The detergent was gradually removed, and proteoliposomes were formed by multiple additions of Biobeads SM (Bio-Rad). The proteoliposomes were separated from the Biobeads, collected by centrifugation, resuspended to a final concentration of 10 mg/ml lipid with appropriate luminal solution, snap frozen and stored at -80°C . If the need arose to change the internal solution, the proteoliposomes were collected by centrifugation, diluted in the desired solution, freeze-thawed three times and extruded.

Transport assays

Prior to performing the transport assays, the proteoliposomes were extruded through a 400 nm filter and concentrated to 100 mg/ml lipid by centrifugation. A typical transport assay was performed thus; the transport reaction was started by 150-fold dilution of the proteoliposomes into appropriate reaction solution warmed to 30°C . The reaction solution varied depending on the experiment (see below for details), but for a typical transport assay this solution consisted of 20 mM Tris/HEPES, pH 7.5, 100 mM KCl, 100 mM NaCl, 1 μM valinomycin and 1 μM [^3H]-succinate (American Radiolabeled Chemicals). For all transport assays performed, at each timepoint, a 0.2 ml sample was taken and diluted 10-fold in ice-cold quench buffer consisting of 20 mM Tris/HEPES, pH 7.5 and 200 mM choline chloride (ChCl). The quenched reaction was then subjected to rapid filtration over a nitrocellulose membrane (Millipore, 0.22 μm) and the filters were washed with 3 ml of quench buffer. Each filter was dissolved in FilterCount liquid scintillation cocktail (PerkinElmer) and associated radioactivity was counted using a Trilux beta counter (PerkinElmer).

The composition of the solutions was changed depending on the requirements of the experiment. In the cation dependence experiment (Fig. 2), valinomycin was omitted and the Na⁺ in the internal and external solutions was replaced with LiCl or KCl. ChCl was used to maintain the ionic and osmotic balance of the solutions. In the Na⁺ dose response experiment (Fig. 3), the internal solution contained 20 mM Tris/HEPES, pH 7.5, 1 mM NaCl and 200 mM KCl and 99 mM ChCl. The external solution consisted of 20 mM Tris/HEPES, pH 7.5, 100 mM KCl, 2.5-300 mM NaCl, 1 μM valinomycin and 1 μM [³H]-succinate. The kinetic parameters were derived by fitting the data with the Hill equation;

$$V = \frac{V_{max}[S]^b}{[K_{(0.5)}]^b + [S]^b}$$

where [S] is the substrate concentration and b is the Hill coefficient.

For the succinate dose response curve (Fig. 6A), the kinetic parameters were derived by fitting the data with the Hill equation and Michaelis-Menten equation;

$$V = \frac{V_{max}[S]}{K_m + [S]}$$

For the pH dependence experiments (Fig. 7), transport assays were performed as detailed for the typical transport assay. The low pH values (pH 4-5) of the solutions were attained using and Tris/aspartate buffering system, the pH values of the rest were set with Tris/MES buffering system. For the electrogenicity experiment (Fig. 4B), we set the different voltages across the membrane by varying the K⁺ gradient across the membrane in the presence of valinomycin; -102.2 mV (100 mM_{IN}/1 mM_{OUT}), -49.6 mV (100 mM_{IN}/15 mM_{OUT}), 0 mV (100 mM_{IN}/100 mM_{OUT}), 49.6 mV (15 mM_{IN}/100 mM_{OUT}), and 102.2 mV (1 mM_{IN}/100 mM_{OUT}). For the counterflow assay (Fig. 5), the liposomes were loaded with 50 mM Tris/HEPES, pH 7.5, 100 mM NaCl, and 1 mM succinate. The external solution contained 50 mM Tris/HEPES, pH 7.5, 100 mM NaCl, 900 nM succinate, and 100 nM [³H]-succinate. This experiment was also performed in the absence of Na⁺ ions, in which case the NaCl in the above solutions was replaced with ChCl. For the citrate dose response experiment (Fig. 8C), trisodium citrate was used to increase

the concentration of citrate in the external solution. The Na⁺ concentration and ionic balance was maintained by addition of NaCl. The osmotic balance of the solutions was maintained using sucrose. The percentage abundance of the various citrate and succinate protonation states was calculated using HySS2009 software (Alderighi et al., 1999).

Fluorescent labeling of single cysteine mutants

To specifically label only internal cysteines (those facing the lumen of the liposome), proteoliposomes containing VcINDY mutants were first incubated with the membrane impermeable cysteine-reactive reagent methyl-PEG₁₂-maleimide (MM(PEG)12, Thermo Scientific) for 20 minutes at room temperature to fully label external cysteine residues. The MM(PEG)12 reaction was quenched by addition of 100 mM L-cysteine. Excess cysteine and MM(PEG)12 were removed by two washing steps, in which the proteoliposomes were pelleted by centrifugation and resuspended in buffer devoid of the unwanted reagents. The proteoliposomes were solubilized in 2.6 % (w/v) DM and internal cysteine residues were fluorescently labeled by incubation with Alexa Fluor® 488 C5 Maleimide (Life Technologies) for 2 hours at room temperature in a solution comprised of 20 mM Tris/HEPES pH 7.4, 199 mM KCl and 1 mM NaCl. As a positive control and to obtain a “100% labeled” sample, the initial MMPEG12 protection step was excluded. Thus, following DM solubilization, all cysteines were available to fluorescently label. Proteoliposomes were run on SDS-PAGE gels and fluorescently labeled protein was visualized by UV transillumination using Fluorchem E (Proteinsimple). Equal protein loading was ensured by subsequently staining the gels with Coomassie Brilliant Blue dye.

Results

Functional reconstitution of VcINDY

To assess the transport characteristics of VcINDY, we purified the protein, reconstituted it into liposomes, and measured its transport characteristics. We purified detergent-solubilized VcINDY with a single immobilized metal affinity chromatography (IMAC) step using the N-terminal decahistidine tag (Fig. 1), subsequently removing the affinity tag and reconstituting the protein by adding it to Triton X100-destabilized liposomes using the procedure established by Rigaud *et al* (Levy *et al.*, 1992). SDS-PAGE analysis of the resulting proteoliposomes reveals a single band at the same molecular weight as the protein purified in detergent solution (Fig. 1), confirming incorporation of the protein. Given the results of cell-based assays (Mancusso *et al.*, 2012), we initially assessed function by measuring succinate uptake in our reconstituted system. Upon application of an inwardly-directed Na^+ gradient (100 mM outside, 1 mM inside), we observe rapid accumulation of the radiolabeled succinate into the lumen of the proteoliposomes (Fig. 2A, closed circles). Under the same conditions, we find no accumulation of substrate for empty liposomes (data not shown) demonstrating that, as expected, VcINDY is responsible for catalyzing succinate transport. VcINDY-containing proteoliposomes did not accumulate substrate in the presence of equimolar concentrations of Na^+ on both sides of the membrane, revealing that a Na^+ gradient is required for succinate transport (Fig. 2A and B, open triangles).

Cation specificity of succinate transport by VcINDY

All currently characterized members of the DASS family of transporters utilize an electrochemical Na^+ gradient to power transport of their respective substrates, with the exception of fly DrINDY and a vacuolar homolog from *Arabidopsis* (AttDT), both of which are cation independent (Inoue *et al.*, 2002a; Knauf *et al.*, 2002; Emmerlich *et al.*, 2003). Li^+ has been shown to substitute for Na^+ in transport in some

cases or to actually inhibit transport in others, the best example of this being the rat and human orthologs of NaCT; the former is inhibited, whereas the latter is capable of Li⁺-driven transport (Inoue et al., 2003). Previous whole cell transport assays suggest that VcINDY can efficiently couple transport of succinate to both Na⁺ and Li⁺ (at a concentration of 5 mM), but not K⁺ (Mancusso et al., 2012). Our purified, reconstituted system is ideal for rigorously determining ion dependence, as it is free of native transport proteins that might lead to spurious results. As noted, we observe rapid accumulation of succinate upon application of an inwardly-directed Na⁺ (Fig. 2A, closed circles). Replacing Na⁺ with Li⁺ results in measurable, but vastly decreased transport that is only appreciable if plotted separately from the Na⁺ dependent transport (Fig. 2B, open circles). This result is surprising considering the above *in vivo* transport data that suggests almost equal efficacy of the two cations (Mancusso et al., 2012). Note though that those experiments were at much lower [Li⁺] than ours and that strong concentration-dependence of transport to Li⁺ has previously been observed for other SLC13 proteins (Pajor, 2006). We observe no transport activity upon application of a K⁺ gradient, demonstrating that K⁺ is incapable of supporting transport via VcINDY (Fig 2B, closed triangles).

Na⁺ dependence of succinate transport

The number of Na⁺ ions coupled to transport varies among the members of the DASS family; most couple the transport of their respective substrate to 3 Na⁺ ions (Busch et al., 1994; Kekuda et al., 1999; Wang et al., 2000; Dawson et al., 2005; Miyauchi et al., 2006), whereas some couple transport to 2 Na⁺ ions (Markovich et al., 2005; Hall and Pajor, 2007; Pajor et al., 2013), and some to 4 (Inoue et al., 2002c). We investigated the number of Na⁺ ions coupled to succinate transport by VcINDY by monitoring the transport rate of [³H]-succinate in the presence of varying external concentrations of Na⁺. The succinate transport rate depends strongly on the external Na⁺ concentration and shows sigmoidal [Na⁺] dependence, indicative of multiple, cooperative Na⁺ binding sites (Fig. 3). At 30 °C, kinetic analysis revealed a K_m for Na⁺ of 41.7 ± 26 mM, a V_{max} of 53.5 ± 7.2 nmol/mg/min and a Hill coefficient

of 3.2 ± 0.3 (at 1 μM succinate), suggesting 3 or more Na^+ ions are coupled to the transport of one succinate molecule. If indeed VcINDY couples the transport of 1 succinate to 3 (or more) Na^+ ions, we would expect net positive charge movement across the membrane during the transport cycle. The ensuing generation of an inside-positive membrane potential would inhibit further transport of [^3H]-succinate. Under these circumstances, dissipation of this voltage using the K^+ ionophore valinomycin in the presence of K^+ should increase the initial succinate transport rate (given the lack of K^+ -dependence of transport). Indeed, addition of valinomycin resulted in a 2.5-fold increase in the initial rate of succinate transport, demonstrating that transport by VcINDY is electrogenic (Fig. 4A). Furthermore, setting the membrane potential to values between -100 and +100 mV using K^+ /valinomycin reveals variation in transport rates with the applied voltage (Fig. 4B). We observed the highest transport rates at large negative membrane potentials, lower rates at intermediate voltages, and the lowest rates at positive membrane potentials (Fig. 4B). Together, these data demonstrate that transport of succinate is electrogenic and that at least one net positive charge is transferred into the liposome per transport cycle, suggesting that at least 3 Na^+ ions are coupled to transport of 1 succinate molecule per transport cycle.

The exchange reaction in a transporter monitors the binding of substrate and the outward facing to inward facing transition of the protein (Mulligan and Mindell, 2013). In theory, coupling between substrates (in a symporter like VcINDY) requires that only the empty or fully-loaded transporter should be able to efficiently exchange between inward-facing and outward-facing states, otherwise coupling would be compromised (Stein, 1986). Thus, the exchange reaction should require both coupled ions and substrate (the empty transporter, of course, will not mediate exchange of anything). We tested this prediction for VcINDY using a solute counterflow assay to monitor succinate exchange in the presence and absence of equimolar [Na^+] across the membrane (substituting with the non-transportable cation, choline). In this assay, the proteoliposomes are first loaded with a high concentration of unlabeled substrate and then diluted into an external solution containing a trace

amount of [³H]-succinate. Stochastic, alternate sampling of the substrate binding site to both sides of the membrane results in exchange of unlabeled substrate on the inside for radiolabeled substrate on the outside, resulting in uptake of the labeled substrate even without net change in its concentration (Kaczorowski and Kaback, 1979). Over time, however, the substrate gradient will itself drive the transporter, causing net efflux of both hot and cold substrate (and Na⁺) from the liposome until equilibrium is reached. In the presence of 100 mM Na⁺ on both sides of the membrane, VcINDY catalyzes accumulation [³H]-succinate (Fig. 5, note that we terminated the experiment before observing the falling phase of counterflow). However, we observe no exchange activity when Na⁺ is replaced with choline. This result underscores the tight coupling of transport and supports a model where both Na⁺ and succinate are simultaneously bound during substrate translocation, consistent with suggestions from the VcINDY crystal structure. Notably, a previously characterized bacterial ortholog of VcINDY, SdcS from *Staphylococcus aureus* reportedly catalyzes Na⁺-independent exchange of its substrate across the membrane, despite also being a Na⁺ gradient-driven transporter (Hall and Pajor, 2007). If supported by further experiments this finding may yield insight into the nature of the coupling mechanism.

Substrate specificity and kinetics of VcINDY

To explore the interaction between VcINDY and succinate, we monitored the succinate dose dependence of the initial transport rates in the presence of saturating (100 mM) concentrations of Na⁺ (Fig. 6A). This relation is well-fit by a hyperbolic curve, consistent with a single succinate binding site per protomer. The parameters of the fit include K_m of $1.0 \pm 0.2 \mu\text{M}$, V_{max} of $232.6 \pm 17.2 \text{ nmol/mg/min}$, and Hill coefficient of 0.88 ± 0.13 (30 °C and a [Na⁺] of 100 mM), and a turnover rate (K_{cat}) of 1.6 min^{-1} . This number represents a lower limit for the actual turnover rate but is accurate if all protein added to the reconstitution is active and is incorporated into liposomes and the vesicles are tight (Fig. 6A). Combined, these results are consistent with the presence of a non-cooperative succinate binding site

and hint that the motions of the two protomers comprising the dimer are, to a first approximation, independent of one another.

Previous characterization of a few candidate VcINDY substrates suggests that the transporter is capable of transporting succinate and at least interacting with malate and fumarate (Mancusso et al., 2012). Citrate confers enhanced thermostability (compared to the presence of no substrate) and is thought to be responsible for the electron density in the binding site of the crystal structure (Mancusso et al., 2012). We explored the substrate specificity of VcINDY using a competition assay in which we measured the transport of [^3H]-succinate (1 μM) in the presence of excess concentrations (1 mM) of 29 candidate substrates (Fig. 6B). Inhibition of succinate transport implies an interaction between the transporter and the potential substrate. Although an alternative mechanism for inhibition, such as allosteric regulation, cannot be excluded based on this simple assay, the chemical similarity of the candidates to succinate makes a competitive inhibition mechanism seem likely. Furthermore, this experiment does not allow us to discriminate between the inhibitors merely binding to VcINDY versus being transported by the protein. We observe inhibition of succinate transport in the presence of the C_4 -dicarboxylates, succinate, malate, fumarate and oxaloacetate (Fig. 6C); succinate derivatives, 2,3-dimercaptosuccinate and mercaptosuccinate (but interestingly, not 2,3-dimethylsuccinate); and the C_5 -dicarboxylate, α -ketoglutarate. The binding site is clearly sensitive to the length of the carbon chain as neither shorter (oxalate (C_2) and malonate (C_3)) nor longer (glutarate (C_5), adipate (C_6), pimelate (C_7), suberate (C_8)) dicarboxylates substantially inhibit succinate transport (Fig. 6B). Maleate, the *cis* isomer of trans-butenedioic acid, has no inhibitory effects, unlike the *trans* isomer, fumarate, showing that the transporter is isomer selective, a characteristic shared by other DASS members (Kekuda et al., 1999; Wang et al., 2000; Inoue et al., 2002a; Inoue et al., 2002c; Fei et al., 2003). We observe no inhibition by known substrates of NaS1 or NaS2 families; sulfate, selenate, thiosulfate or dimercaptopropane-1-sulfonate (Busch et al., 1994; Markovich et al., 2005). Nor do we find inhibition of succinate transport by aspartate or glutamate, both of which interact with a number

of DASS family members (Chen et al., 1998; Kekuda et al., 1999; Pajor and Sun, 2000; Wang et al., 2000; Strickler et al., 2009; Pajor et al., 2013).

We also tested the inhibitory effect of a number of known DASS family inhibitors. Benzylpenicillin, which inhibits a NaDC3 homolog from Winter Flounder (Burckhardt et al., 2004), elicits no response when added to the transport reaction. Folate, though itself not a substrate of NaDC3, can modulate succinate-derived transport current (Burckhardt et al., 2005); in our hands, folate has a modest inhibitory effect on VcINDY transport. Flufenamic acid yields substantial inhibition of VcINDY transport (Fig. 6B). This compound non-competitively inhibits both eukaryotic and bacterial DASS members (Burckhardt et al., 2004; Pajor and Sun, 2013), suggesting that the binding site for this particular inhibitor is preserved, despite the evolutionary distance between these transporters. Tricarallylate, a tricarboxylate similar in structure to citrate, inhibits transport. Citrate itself, however, does not inhibit transport at 1 mM under these conditions (Fig. 6B, though see below for further assessment of high citrate concentrations).

pH dependence of succinate transport

Determining the charged state of the transported substrate is a key step in understanding the mechanism of VcINDY. Whether the substrate is neutral, singly, or doubly charged (or more than one of these) will affect the ability of the succinate to coordinate cotransported cations, influence the pH dependence of the transporter, and influence the coupling of transport to the membrane potential (via the net charge movement per transport cycle). Since, succinate is a dicarboxylic acid with pKas within the range of pHs tested (4.21 and 5.64), the relative abundance of each protonation state of succinate varies with pH (Fig. 7A-D, solid lines). By examining transport rates at varying external pHs, we can thereby control, to some extent, the relative fractions of the three charged forms of the substrate. While maintaining a pH_{INT} 7.5, we observe that decreasing the pH_{EXT} from 7.5 to 5.5 decreases the transport rate, which (in this range) matches exactly the decrease in the relative

abundance of fully deprotonated succinate (Succ^{2-} ; Fig. 7A, gray line), suggesting that succ^{2-} is the actual substrate of VcINDY. At lower pHs (4-5), the correlation between succinate accumulation rates and relative abundance of fully deprotonated succinate diverges with more substrate accumulating in the liposomes than predicted by the titration curve (Fig. 7A). What is the cause of this divergence? One possibility is that there is proton-driven transport that is only observable at low pHs, unlikely given the lack of gradient dependence at higher pH. Alternatively, there could be a relative increase in the abundance of the mono- and fully-protonated states of succinate (SuccH^{1-} and SuccH_2 , respectively); at low pH, both of these, particularly the neutral form, are known to traverse the lipid bilayer itself (Kaim and Dimroth, 1998, 1999; Janausch et al., 2001). Upon internalization, the higher internal pH in the liposomes (7.5) would fully deprotonate SuccH^{1-} and SuccH_2 , trapping them and resulting in their accumulation. We tested this hypothesis by monitoring accumulation of $[\text{}^3\text{H}]$ -succinate into protein-free liposomes with an internal pH of 7.5 and varying the external pH between 4 and 7.5 (Fig. 7D). At low external pH values we observe substantial accumulation of succinate, accumulation which increases as the external pH decreases. This result validates the second hypothesis, that the deviation from predicted transport rates is due to direct membrane permeability of at least the neutral form of succinate and possibly its singly charged form as well. Indeed, the effects of the permeable succinate protonation states are also seen with fixed external pH 7.5 and varying internal pH. Though we observe robust transport at the higher internal pH, lowering the internal pH favors the membrane-permeant species and they diffuse out of the liposomes, manifesting as an apparent lack of transport (Fig. 7C). These results clearly demonstrate that only the doubly charged protonation state of succinate is transported by VcINDY. Our pH-dependence experiments also reveal that VcINDY transport of succinate is not coupled to a proton gradient since the pH dependence of transport is essentially identical in the absence (Fig. 7B) or presence of an inwardly directed (Fig. 7A) or outwardly directed (Fig. 7C) pH gradient (when we neglect the effects of direct succinate bilayer permeability).

Investigating the interactions between VcINDY and citrate

In our substrate competition assay, we observed no inhibition of succinate transport in the presence of 1 mM citrate (Fig. 6B), a surprising result given the presumed citrate density in the crystal structure and the stabilizing effect of the ion on the folded protein (Mancusso et al., 2012). Comparing our transport conditions to those of crystallization, we found that the VcINDY was crystallized (in 100 mM citrate) at pH 6.5, whereas our competition assay was performed at pH 7.5. At pH 7.5, citrate is predominantly in its deprotonated state, citrate³⁻, whereas, at pH 6.5, half the citrate is citrate³⁻, while the other half is citrateH²⁻ (Fig. 8A, green and yellow block colors, respectively). Perhaps VcINDY only binds doubly charged anions, as we demonstrated is the case with succinate, which would explain why we observe no inhibition by citrate at pH 7.5 where the citrateH²⁻ protonation state is scarce. To test this, we monitored the transport of succinate in the presence of excess (1 mM) citrate at pH 7.5, pH 6.5 and pH 5.5. At pH 7.5, both succinate and citrate will be almost fully deprotonated (Fig. 8A, citrate, block colors; succinate, line data). At pH 6.5, however, a large population of citrate is dianionic and the majority of succinate is still deprotonated. At pH 5.5, approximately 80% of the citrate will be dianionic, whereas 50% of the deprotonated succinate will remain. If citrateH²⁻ binds and inhibits succinate transport by VcINDY, then lowering the pH should lead to observable inhibition. At the 3 different pH values, we observe no inhibitory effects of citrate on succinate transport, indicating that at this citrate concentration (1 mM) neither citrate³⁻ nor citrateH²⁻ interacts with VcINDY (Fig. 8B). We investigated whether citrate simply binds at much lower affinity by measuring succinate transport in the presence of increasing external concentrations of citrate. At pH 7.5, we observe 25% inhibition of transport activity at 75 mM citrate, the highest concentration we tested (Fig. 8C, closed circles). At pH 5.5, where the dianionic form of citrate is most abundant, we observe no inhibitory effects of citrate at 10 mM, however, increasing the citrate concentration to 25 mM results in approximately 60% inhibition of succinate transport (Fig. 8C, open circles). Further increases in citrate concentration do not result in further inhibition (Fig. 8C). Increased inhibition by citrate at the lower pH suggests that

citrateH²⁻ does indeed interact with VcINDY, albeit with low affinity. Why do we see ~40% residual transport activity? If citrate is a competitive inhibitor that binds to VcINDY at the same site as succinate, one would expect complete inhibition of VcINDY transport activity upon adding sufficient excess of the ion. The fact that we do not see complete inhibition has a potentially simple explanation; if, as has been suggested (Mancusso et al., 2012), citrate is an inward-facing state specific inhibitor of VcINDY then its inhibitory efficacy would be dependent on the orientation of VcINDY in the membrane. If the orientation of VcINDY in the liposomes is mixed, i.e. VcINDY is present in the membrane in two populations; outside out (as it is oriented *in vivo*) and inside out, then citrate would only affect the population of VcINDY with its inner façade facing outward.

We addressed this issue by determining the orientation of VcINDY in the liposome membrane. We introduced single cysteine residues into a cysteine-less version of VcINDY (cysless, each native cysteine was mutated to serine) at positions on either the cytoplasmic (A171C) or extracellular (V343C) faces of the protein (Fig. 9A). Cysless VcINDY and the two single cysteine mutants display measurable transport activity upon reconstitution into liposomes (Fig. 9B). Because our fluorescent probe is somewhat membrane permeant (data not shown), we designed a multistep protocol to establish protein orientation. We treated all three mutants with the membrane impermeable, thiol-reactive reagent, methyl-PEG₁₂-maleimide (MM(PEG)12), solubilized the membrane, and labeled the remaining cysteines with the thiol-reactive fluorophore, Alexa488-maleimide. We analyzed the extent of labeling by separating the proteins using polyacrylamide gel electrophoresis and imaging the gels while exciting the fluorophore with UV transillumination. Thus, only cysteine residues facing the lumen of the proteoliposomes, protected from MM(PEG)12 labeling, should be fluorescently labeled. The reactivity pattern of the two single cysteine mutants suggests VcINDY adopts a mixed orientation in the membrane (Fig. 9C). First, both the internal site (V171C) and the external site (A343C) exhibit fluorescent labeling (Fig. 9C, Lane 1 for each mutant), indicating that both cysteines, despite being on opposite faces of the protein, were at least partially protected from MM(PEG)12 modification prior to

membrane solubilization. Solubilizing the membrane prior to MM(PEG)12 labeling results in no fluorescent labeling (Fig. 9C, Lane 2); therefore we are indeed fluorescently labeling the internally located cysteines. Secondly, excluding the MM(PEG)12 labeling step, solubilizing the membrane and fluorescently labeling all available cysteines results in substantially greater fluorescent labeling (Fig. 9C, Lane 3), demonstrating that each cysteine, regardless of its position on the protein can be exposed to either side of the membrane. These data reveal that the VcINDY protein incorporates in the liposome membrane in both possible orientations. Though our data are not quantitative enough to accurately determine the relative proportions of these orientations, they are consistent with a roughly equal distribution of both. In this context, our results on citrate inhibition are at least consistent with a sided mechanism of inhibition.

Does VcINDY have an uncoupled chloride conductance?

The VcINDY protomer is composed of two distinct domains; the scaffold domain, which forms all of the contacts at the dimer interface, and the transport domain, which houses all of the substrate binding residues (Mancusso et al., 2012). This architecture is reminiscent of the EAAT homolog, Glt_{ph}, whose structure and mechanism have been well studied (Yernool et al., 2004; Reyes et al., 2009; Hanelt et al., 2013; Jensen et al., 2013). During its transport cycle, Glt_{ph} undergoes an elevator-type movement of the transport domain relative to the immobile scaffold domain (known as the trimerization domain in Glt_{ph}), exposing the binding site from one side of the membrane to the other. Due to the architectural similarity between VcINDY and Glt_{ph} there is a possibility that they share a similar mode of action, namely, an elevator-type mechanism. A characteristic of the EAATs and Glt_{ph} is the presence of an uncoupled anion conductance, the pathway of which has been proposed to be located at the interface between the transport domain and the scaffold (Ryan and Mindell, 2007; Verdon and Boudker, 2012). If an uncoupled Cl⁻ conductance is a consequence of an elevator-like mechanism, this uncoupled anion conductance may also be shared. A number of other DASS family members have

been shown to exhibit interesting traits in the presence of anions, although not necessarily suggestive of an uncoupled chloride conductance (Inoue et al., 2002a; Oshiro and Pajor, 2005).

As we previously described, VcINDY-mediated transport of succinate is electrogenic: transport is enhanced by dissipating the membrane potential, as by valinomycin in Figure 4. If VcINDY also carries an uncoupled Cl⁻ conductance, then Cl⁻ ion would also aid in dissipating the membrane potential, thereby facilitating transport. This effect should only be apparent in the absence of valinomycin/K⁺. In this case, replacing Cl⁻ with an impermeant anion should reduce transport rates, but only in the absence of valinomycin (Fig. 4), as was the case for GlT_{ph} (Ryan and Mindell, 2007). We initially replaced chloride with gluconate and found, unexpectedly, that 100 mM gluconate is an excellent inhibitor of VcINDY (data not shown), despite exhibiting no inhibitory properties at lower concentrations (Fig. 6B). We therefore substituted gluconate with another commonly used impermeable anion, methanesulfonate. In the absence of valinomycin, we observe more inhibition when the chloride is replaced with methanesulfonate (Fig. 10), similar to what we would expect upon Cl⁻ replacement in GlT_{ph}. However, in the presence of valinomycin, where any inhibitory electrical potential should be completely dissipated, we still see this inhibition, and importantly the fraction of transport remaining is identical to that exhibited in the absence of valinomycin (Fig. 10). This contrasts strongly with the observations reported for GlT_{ph}, where addition of valinomycin fully compensates for the inhibition caused by Cl⁻ replacement (Ryan and Mindell, 2007). These data suggest that the inhibition observed in the absence of valinomycin is caused by the presence of methanesulfonate rather than the absence of chloride. This result therefore indicates that VcINDY does not have an uncoupled chloride conductance. However, it does further demonstrate that VcINDY is capable of interacting with a number of structurally unrelated anions.

Discussion

The crystal structure of VcINDY represents the only high resolution structural information available for the DASS family of transporters. This study reports on the functional reconstitution and characterization of VcINDY to establish which transport features it shares with other DASS family members, including the physiologically important SLC13 family from humans. A detailed understanding of the transport mechanism of VcINDY will allow us to begin to understand the functional characteristics of other DASS family members from a structural viewpoint.

In accordance with the majority of functionally characterized DASS family members, VcINDY utilizes an electrochemical Na^+ gradient to power transport of the model substrate, succinate. A Li^+ gradient can substitute for the Na^+ gradient at 100 mM, but with a much lower relative efficacy compared to what was seen in cell based assays at 5 mM Li^+ (Mancusso et al., 2012). This observed disparity between cell-based and liposome based assays is likely due to complications that arise from measuring transport in whole cells where the internal solution composition is hard to control and there are unknown contributions from endogenous transporters; as opposed to a purified and reconstituted system where a single protein is present and altering and maintaining the reaction solutions is trivial. The structure of VcINDY suggests a single substrate binding site per protomer (Mancusso et al., 2012). This assertion is corroborated by kinetic analysis of succinate transport that revealed a hyperbolic dose response curve and a Hill coefficient of 0.88, consistent with a single, non-cooperative binding site for succinate. Under similar experimental conditions, although performed in whole cell assays or in membrane vesicles, two related bacterial transporters, SdcF and SdcS (30% and 32% identical to VcINDY, respectively), have sigmoidal dose response curves, indicative of cooperative transport activity (Pajor and Sun, 2013; Pajor et al., 2013). This finding suggests that either two substrate molecules bind to the same protomer, a notion inconsistent with our current structural understanding of this transporter family; or, the two protomers in a VcINDY dimer act cooperatively. Again, this

observed sigmoidal activity may be a consequence of using whole cells and membrane vesicles in transport assays, as opposed to the purified and reconstituted system. Adding weight to this argument is the observation that purified and reconstituted SdcS has a Hill coefficient of 0.83, more in keeping with the apparently non-cooperative transport we observe for VcINDY (Hall and Pajor, 2007). Although we cannot completely rule out cooperativity between the subunits, our work points to each protomer working independently.

The transport data presented here is inconsistent with a H^+ gradient contributing to transport, however, we found transport of succinate to be highly pH dependent. This mirrors the observations of pH-dependent transport for NaDC1 in whole cells (Wright et al., 1982). The decrease in succinate transport as pH dropped corresponds almost perfectly with the decrease in the theoretical abundance of succinate²⁻ at higher pH, strongly suggesting that succinate²⁻ is the actual substrate of VcINDY. In contrast, succinate transport by NaDC1 was completely insensitive to the solution pH, suggesting that the mono- and deprotonated forms of succinate may both be transported (Pajor, 1995). NaDC3, however, is highly pH-dependent, showing clearly that succinate²⁻ is the only succinate protonation state transported (Kekuda et al., 1999). Of the other bacterial DASS members where the pH dependence of succinate transport has been studied; SdcL from *Bacillus licheniformis* was insensitive to pH (although the pH range tested was limited) (Strickler et al., 2009), and SdcS was sensitive demonstrating that succinate²⁻ is the preferred substrate here as well (Hall and Pajor, 2005). The protonation state of the substrate has profound effects on the transport mechanism as it is fundamentally linked to the number of coupling ions transported and the electrogenicity of the transporter. The observation that succinate²⁻ is the preferred protonation state, coupled with the fact that transport by VcINDY was electrogenic demonstrates that at least 3 Na^+ ions are coupled to the transport of one succinate²⁻. This stoichiometry is corroborated by kinetic analyses of both succinate and Na^+ dose response curves that revealed Hill coefficients of 0.88 and 3.0, respectively. Though strictly these results establish 3 as the lower limit of the number of Na^+ ions, we suggest that the

coupling stoichiometry is indeed three, consistent with the Hill coefficient and by analogy to other coupled transporters. Almost all of the DASS family members have a substrate:coupling ion stoichiometry of 1:3 (Busch et al., 1994; Chen et al., 1998; Kekuda et al., 1999; Miyauchi et al., 2006). The two exceptions are NaCT, which couples the transport of both citrate³⁻ and succinate²⁻ to 4 Na⁺ ions (Inoue et al., 2002c), and all currently characterized bacterial homologs. Aside from VcINDY, all other bacterial homologs co-transport 2 Na⁺ ions with succinate in an electroneutral process (Hall and Pajor, 2005, 2007; Strickler et al., 2009; Pajor et al., 2013). Of all the bacterial transporters characterized to date, VcINDY is the most functionally similar to the eukaryotic homologs and is therefore an excellent choice for a bacterial model of this family.

Aside from its apparent inability to transport citrate, the mechanism (electrogenicity, coupling ion stoichiometry) and substrate specificity of VcINDY most resembles the eukaryotic DASS members NaDC1 and NaDC3. The primary functional distinction between NaDC1 and 3 is their K_m values; the former is considered low affinity with a K_m ranging from 300-750 μ M, and the latter is considered high affinity with a K_m range of 2-20 μ M. With a K_m value of 1 μ M (the lowest K_m value reported for this family), VcINDY is most functionally similar to NaDC3 in this regard.

Our data suggests that citrate is capable of binding VcINDY, but only in its dianionic form and possibly only to one side of the protein. The first part of this conclusion is based on the observation that succinate transport is mainly affected by the presence of citrate at pH 5.5, where the majority of the citrate is dianionic, as opposed to pH 7.5, where the citrate³⁻ is the predominant protonation state. In keeping with this, the crystal structure of VcINDY was captured at pH 6.5, where a large proportion of the 50 mM citrate present would be dianionic and therefore available to bind (Mancusso et al., 2012). However, inconsistent with this proposition is the observation that citrate confers considerable thermostability to VcINDY in pH 8 conditions, where only a small proportion of the citrate would be dianionic (Mancusso et al., 2012). This stabilizing effect may be explained by an allosteric interaction with citrate, but further work will be required to resolve this issue. Based on the crystal structure alone,

citrate was proposed to be an inward-facing state inhibitor of VcINDY (Mancusso et al., 2012). Our results are consistent with this claim: we observed maximal inhibition of 50% regardless of how high we increased the citrate concentration and we also demonstrate that the orientation of VcINDY in the liposomes is mixed. Further work is required to fully elaborate on the interaction between VcINDY and citrate. To date, VcINDY is the only bacterial DASS member to demonstrably interact with citrate (Hall and Pajor, 2005, 2007; Youn et al., 2008; Strickler et al., 2009; Pajor et al., 2013). The observed interaction with citrate²⁻, though not actual transport, further strengthens the functional similarity between VcINDY and NaDC1 and 3, both of which transport citrate and prefer the doubly charged form (Kekuda et al., 1999; Wang et al., 2000). NaCT, on the other hand, transports the trianionic form of citrate (Inoue et al., 2002b; Inoue et al., 2002c; Inoue et al., 2004).

Although our functional assays lack the resolution to dissect the order of substrate binding, we can suggest the following simple transport scheme based on extrapolation from other Na⁺-dependent transporters (Fig. 11); 1) VcINDY, in the outward-facing state binds 1-3 Na⁺ ions, which induces formation of a favorable binding site for succinate²⁻, which binds, followed by any remaining Na⁺ ions; 2) VcINDY reorients from the outward-facing state to the inward-facing state (a conformation that resembles the current crystal structure), presumably via an occluded state; 3) Na⁺ ion and succinate are released in an unknown order, 4) empty transporter reorients back to the outward-facing state to begin the cycle anew. Specific predictions of such an ordered mechanism can be tested experimentally in the future.

The coupling of succinate transport to 3 Na⁺ ions is advantageous to both *V. cholerae*, who use succinate as a nutrient, and in the other physiological settings DASS family members are found. As succinate is transported in its divalent form, co-transport of 3 (or more) Na⁺ ions makes the process electrogenic, allowing the negative membrane potential to help drive transport in addition to the Na⁺ gradient. When the transport process reaches equilibrium, the final succinate concentration in the cell

will be proportional to the cube of the Na⁺-gradient, namely, $([Na^+]_{out}/[Na^+]_{in})^3$ (Stein, 1986), much higher than that a co-transporter with a Na⁺-substrate ratio of 1 or 2 can possibly achieve.

The functional characterization of VcINDY presented here lays the groundwork to bridge the gap between the structural insight gained from this bacterial transporter and the function of its eukaryotic counterparts. Our results are also essential prerequisites for any computational examinations of binding or transport in VcINDY. This work demonstrates that many of the functional properties of physiologically relevant DASS family members are retained in VcINDY, making it an excellent model for future structural and mechanistic studies on this family of transporters.

Acknowledgements

We thank Dr. Romina Mancusso for helpful discussions, Jinmei Song and Bining Lu for preliminary experiments in whole cells, and Lucy Forrest and Kenton Swartz for critical readings of the manuscript. This work was supported by the Intramural Research Program of the NIH, NINDS, and NIH grants (R01-DK073973, R01-GM093825 and U54-GM095315).

Reference list

- Alderighi, L., P. Gans, A. Ienco, D. Peters, A. Sabatini, and A. Vacca. 1999. Hyperquad simulation and speciation (HySS): a utility program for the investigation of equilibria involving soluble and partially soluble species. *Coordination Chemistry Reviews*. 184:311-318.
- Bergeron, M.J., B. Clemencon, M.A. Hediger, and D. Markovich. 2013. SLC13 family of Na(+)-coupled di- and tri-carboxylate/sulfate transporters. *Molecular aspects of medicine*. 34:299-312.
- Birkenfeld, A.L., H.Y. Lee, F. Guebre-Egziabher, T.C. Alves, M.J. Jurczak, F.R. Jornayvaz, D. Zhang, J.J. Hsiao, A. Martin-Montalvo, A. Fischer-Rosinsky, J. Spranger, A.F. Pfeiffer, J. Jordan, M.F. Fromm, J. Konig, S. Lieske, C.M. Carmean, D.W. Frederick, D. Weismann, F. Knauf, P.M. Irusta, R. De Cabo, S.L. Helfand, V.T. Samuel, and G.I. Shulman. 2011. Deletion of the mammalian INDY homolog mimics aspects of dietary restriction and protects against adiposity and insulin resistance in mice. *Cell metabolism*. 14:184-195.
- Burckhardt, B.C., J. Lorenz, G. Burckhardt, and J. Steffgen. 2004. Interactions of benzylpenicillin and non-steroidal anti-inflammatory drugs with the sodium-dependent dicarboxylate transporter NaDC-3. *Cellular physiology and biochemistry : international journal of experimental cellular physiology, biochemistry, and pharmacology*. 14:415-424.
- Burckhardt, B.C., J. Lorenz, C. Kobbe, and G. Burckhardt. 2005. Substrate specificity of the human renal sodium dicarboxylate cotransporter, hNaDC-3, under voltage-clamp conditions. *American journal of physiology. Renal physiology*. 288:F792-799.
- Busch, A.E., S. Waldegger, T. Herzer, J. Biber, D. Markovich, H. Murer, and F. Lang. 1994. Electrogenic cotransport of Na⁺ and sulfate in *Xenopus* oocytes expressing the cloned Na⁺SO₄⁽²⁻⁾ transport protein NaSi-1. *The Journal of biological chemistry*. 269:12407-12409.
- Chen, C.C., and T.H. Wilson. 1986. Solubilization and functional reconstitution of the proline transport system of *Escherichia coli*. *The Journal of biological chemistry*. 261:2599-2604.

- Chen, X.Z., C. Shayakul, U.V. Berger, W. Tian, and M.A. Hediger. 1998. Characterization of a rat Na⁺-dicarboxylate cotransporter. *The Journal of biological chemistry*. 273:20972-20981.
- Dawson, P.A., K.J. Pirlo, S.E. Steane, K.A. Nguyen, K. Kunzelmann, Y.J. Chien, and D. Markovich. 2005. The rat Na⁺-sulfate cotransporter rNaS2: functional characterization, tissue distribution, and gene (slc13a4) structure. *Pflugers Archiv : European journal of physiology*. 450:262-268.
- Denton, R.M., and P.J. Randle. 1966. Citrate and the regulation of adipose-tissue phosphofructokinase. *The Biochemical journal*. 100:420-423.
- Emmerlich, V., N. Linka, T. Reinhold, M.A. Hurth, M. Traub, E. Martinoia, and H.E. Neuhaus. 2003. The plant homolog to the human sodium/dicarboxylic cotransporter is the vacuolar malate carrier. *Proceedings of the National Academy of Sciences of the United States of America*. 100:11122-11126.
- Fei, Y.J., K. Inoue, and V. Ganapathy. 2003. Structural and functional characteristics of two sodium-coupled dicarboxylate transporters (ceNaDC1 and ceNaDC2) from *Caenorhabditis elegans* and their relevance to life span. *The Journal of biological chemistry*. 278:6136-6144.
- Garland, P.B., P.J. Randle, and E.A. Newsholme. 1963. Citrate as an Intermediary in the Inhibition of Phosphofructokinase in Rat Heart Muscle by Fatty Acids, Ketone Bodies, Pyruvate, Diabetes, and Starvation. *Nature*. 200:169-170.
- Hall, J.A., and A.M. Pajor. 2005. Functional characterization of a Na⁽⁺⁾-coupled dicarboxylate carrier protein from *Staphylococcus aureus*. *Journal of bacteriology*. 187:5189-5194.
- Hall, J.A., and A.M. Pajor. 2007. Functional reconstitution of SdcS, a Na⁺-coupled dicarboxylate carrier protein from *Staphylococcus aureus*. *Journal of bacteriology*. 189:880-885.
- Hanelt, I., D. Wunnicke, E. Bordignon, H.J. Steinhoff, and D.J. Slotboom. 2013. Conformational heterogeneity of the aspartate transporter Glt(Ph). *Nature structural & molecular biology*. 20:210-214.

- Ho, H.T., B.C. Ko, A.K. Cheung, A.K. Lam, S. Tam, S.K. Chung, and S.S. Chung. 2007. Generation and characterization of sodium-dicarboxylate cotransporter-deficient mice. *Kidney international*. 72:63-71.
- Inoue, K., Y.J. Fei, W. Huang, L. Zhuang, Z. Chen, and V. Ganapathy. 2002a. Functional identity of *Drosophila melanogaster* Indy as a cation-independent, electroneutral transporter for tricarboxylic acid-cycle intermediates. *The Biochemical journal*. 367:313-319.
- Inoue, K., Y.J. Fei, L. Zhuang, E. Gopal, S. Miyauchi, and V. Ganapathy. 2004. Functional features and genomic organization of mouse NaCT, a sodium-coupled transporter for tricarboxylic acid cycle intermediates. *The Biochemical journal*. 378:949-957.
- Inoue, K., L. Zhuang, and V. Ganapathy. 2002b. Human Na⁺-coupled citrate transporter: primary structure, genomic organization, and transport function. *Biochemical and biophysical research communications*. 299:465-471.
- Inoue, K., L. Zhuang, D.M. Maddox, S.B. Smith, and V. Ganapathy. 2002c. Structure, function, and expression pattern of a novel sodium-coupled citrate transporter (NaCT) cloned from mammalian brain. *The Journal of biological chemistry*. 277:39469-39476.
- Inoue, K., L. Zhuang, D.M. Maddox, S.B. Smith, and V. Ganapathy. 2003. Human sodium-coupled citrate transporter, the orthologue of *Drosophila* Indy, as a novel target for lithium action. *The Biochemical journal*. 374:21-26.
- Janausch, I.G., O.B. Kim, and G. Uden. 2001. DctA- and Dcu-independent transport of succinate in *Escherichia coli*: contribution of diffusion and of alternative carriers. *Archives of microbiology*. 176:224-230.
- Jensen, S., A. Guskov, S. Rempel, I. Hanelt, and D.J. Slotboom. 2013. Crystal structure of a substrate-free aspartate transporter. *Nature structural & molecular biology*. 20:1224-1226.

- Kaczorowski, G.J., and H.R. Kaback. 1979. Mechanism of lactose translocation in membrane vesicles from *Escherichia coli*. 1. Effect of pH on efflux, exchange, and counterflow. *Biochemistry*. 18:3691-3697.
- Kaim, G., and P. Dimroth. 1998. Voltage-generated torque drives the motor of the ATP synthase. *The EMBO journal*. 17:5887-5895.
- Kaim, G., and P. Dimroth. 1999. ATP synthesis by F-type ATP synthase is obligatorily dependent on the transmembrane voltage. *The EMBO journal*. 18:4118-4127.
- Kekuda, R., H. Wang, W. Huang, A.M. Pajor, F.H. Leibach, L.D. Devoe, P.D. Prasad, and V. Ganapathy. 1999. Primary structure and functional characteristics of a mammalian sodium-coupled high affinity dicarboxylate transporter. *The Journal of biological chemistry*. 274:3422-3429.
- Knauf, F., B. Rogina, Z. Jiang, P.S. Aronson, and S.L. Helfand. 2002. Functional characterization and immunolocalization of the transporter encoded by the life-extending gene *Indy*. *Proceedings of the National Academy of Sciences of the United States of America*. 99:14315-14319.
- Levy, D., A. Gulik, A. Bluzat, and J.L. Rigaud. 1992. Reconstitution of the sarcoplasmic reticulum Ca²⁺-ATPase: mechanisms of membrane protein insertion into liposomes during reconstitution procedures involving the use of detergents. *Biochimica et biophysica acta*. 1107:283-298.
- Love, J., F. Mancina, L. Shapiro, M. Punta, B. Rost, M. Girvin, D.N. Wang, M. Zhou, J.F. Hunt, T. Szyperski, E. Gouaux, R. MacKinnon, A. McDermott, B. Honig, M. Inouye, G. Montelione, and W.A. Hendrickson. 2010. The New York Consortium on Membrane Protein Structure (NYCOMPS): a high-throughput platform for structural genomics of integral membrane proteins. *Journal of structural and functional genomics*. 11:191-199.
- Mancusso, R., G.G. Gregorio, Q. Liu, and D.N. Wang. 2012. Structure and mechanism of a bacterial sodium-dependent dicarboxylate transporter. *Nature*. 491:622-626.

- Markovich, D., R.R. Regeer, K. Kunzelmann, and P.A. Dawson. 2005. Functional characterization and genomic organization of the human Na(+)-sulfate cotransporter hNaS2 gene (SLC13A4). *Biochemical and biophysical research communications*. 326:729-734.
- Miyauchi, S., S.R. Srinivas, Y.J. Fei, E. Gopal, N.S. Umapathy, H. Wang, S.J. Conway, V. Ganapathy, and P.D. Prasad. 2006. Functional characteristics of NaS2, a placenta-specific Na+-coupled transporter for sulfate and oxyanions of the micronutrients selenium and chromium. *Placenta*. 27:550-559.
- Mulligan, C., and J.A. Mindell. 2013. Mechanism of transport modulation by an extracellular loop in an archaeal Excitatory Amino Acid Transporter (EAAT) homolog. *The Journal of biological chemistry*. In Press.
- Oshiro, N., and A.M. Pajor. 2005. Functional characterization of high-affinity Na(+)/dicarboxylate cotransporter found in *Xenopus laevis* kidney and heart. *American journal of physiology. Cell physiology*. 289:C1159-1168.
- Pajor, A.M. 1995. Sequence and functional characterization of a renal sodium/dicarboxylate cotransporter. *The Journal of biological chemistry*. 270:5779-5785.
- Pajor, A.M. 2006. Molecular properties of the SLC13 family of dicarboxylate and sulfate transporters. *Pflugers Archiv : European journal of physiology*. 451:597-605.
- Pajor, A.M. 2013. Sodium-coupled dicarboxylate and citrate transporters from the SLC13 family. *Pflugers Archiv : European journal of physiology*.
- Pajor, A.M., and N. Sun. 1996. Functional differences between rabbit and human Na(+)-dicarboxylate cotransporters, NaDC-1 and hNaDC-1. *The American journal of physiology*. 271:F1093-1099.
- Pajor, A.M., and N.N. Sun. 2000. Molecular cloning, chromosomal organization, and functional characterization of a sodium-dicarboxylate cotransporter from mouse kidney. *American journal of physiology. Renal physiology*. 279:F482-490.

- Pajor, A.M., and N.N. Sun. 2013. Nonsteroidal anti-inflammatory drugs and other anthranilic acids inhibit the Na(+)/dicarboxylate symporter from *Staphylococcus aureus*. *Biochemistry*. 52:2924-2932.
- Pajor, A.M., N.N. Sun, and A. Leung. 2013. Functional Characterization of SdcF from *Bacillus licheniformis*, a Homolog of the SLC13 Na(+)/Dicarboxylate Transporters. *The Journal of membrane biology*. 246:705-715.
- Quick, M., H. Yano, N.R. Goldberg, L. Duan, T. Beuming, L. Shi, H. Weinstein, and J.A. Javitch. 2006. State-dependent conformations of the translocation pathway in the tyrosine transporter Tyt1, a novel neurotransmitter:sodium symporter from *Fusobacterium nucleatum*. *The Journal of biological chemistry*. 281:26444-26454.
- Reyes, N., C. Ginter, and O. Boudker. 2009. Transport mechanism of a bacterial homologue of glutamate transporters. *Nature*. 462:880-885.
- Rogina, B., R.A. Reenan, S.P. Nilsen, and S.L. Helfand. 2000. Extended life-span conferred by cotransporter gene mutations in *Drosophila*. *Science*. 290:2137-2140.
- Ruderman, N.B., A.K. Saha, D. Vavvas, and L.A. Witters. 1999. Malonyl-CoA, fuel sensing, and insulin resistance. *The American journal of physiology*. 276:E1-E18.
- Ryan, R.M., E.L. Compton, and J.A. Mindell. 2009. Functional characterization of a Na⁺-dependent aspartate transporter from *Pyrococcus horikoshii*. *The Journal of biological chemistry*. 284:17540-17548.
- Ryan, R.M., and J.A. Mindell. 2007. The uncoupled chloride conductance of a bacterial glutamate transporter homolog. *Nature structural & molecular biology*. 14:365-371.
- Saier, M.H., Jr., C.V. Tran, and R.D. Barabote. 2006. TCDB: the Transporter Classification Database for membrane transport protein analyses and information. *Nucleic acids research*. 34:D181-186.

- Spencer, A.F., and J.M. Lowenstein. 1962. The supply of precursors for the synthesis of fatty acids. *The Journal of biological chemistry*. 237:3640-3648.
- Stein, W.D. 1986. Transport and Diffusion across Cell Membranes. Academic Press, New York. 306-315 pp.
- Strickler, M.A., J.A. Hall, O. Gaiko, and A.M. Pajor. 2009. Functional characterization of a Na(+)-coupled dicarboxylate transporter from *Bacillus licheniformis*. *Biochimica et biophysica acta*. 1788:2489-2496.
- Verdon, G., and O. Boudker. 2012. Crystal structure of an asymmetric trimer of a bacterial glutamate transporter homolog. *Nature structural & molecular biology*. 19:355-357.
- Wang, H., Y.J. Fei, R. Kekuda, T.L. Yang-Feng, L.D. Devoe, F.H. Leibach, P.D. Prasad, and V. Ganapathy. 2000. Structure, function, and genomic organization of human Na(+)-dependent high-affinity dicarboxylate transporter. *American journal of physiology. Cell physiology*. 278:C1019-1030.
- Wright, S.H., I. Kippen, and E.M. Wright. 1982. Stoichiometry of Na⁺-succinate cotransport in renal brush-border membranes. *J Biol Chem*. 257:1773-1778.
- Yernool, D., O. Boudker, Y. Jin, and E. Gouaux. 2004. Structure of a glutamate transporter homologue from *Pyrococcus horikoshii*. *Nature*. 431:811-818.
- Youn, J.W., E. Jolkver, R. Kramer, K. Marin, and V.F. Wendisch. 2008. Identification and characterization of the dicarboxylate uptake system DccT in *Corynebacterium glutamicum*. *Journal of bacteriology*. 190:6458-6466.

Figure legends

Figure 1 Purification and reconstitution of VcINDY. Crystal structure of VcINDY (PDB accession 4F35) viewed from (A) within the plane of the membrane and (B) perpendicular to the membrane on the periplasmic side. One protomer is colored white and the other is blue. The position of the bound citrate (pink spheres) and Na⁺ ions (green spheres) are shown. (C) SDS-PAGE analysis of VcINDY following IMAC-purification (“Detergent”) and reconstitution into liposomes (“Proteoliposomes”). The band corresponding to VcINDY is labeled. Standard molecular weights (M) are indicated on the left of the gel.

Figure 2 Cation specificity of VcINDY transport. (A) Transport of ³H-succinate into VcINDY-containing liposomes in the presence of an inwardly directed Na⁺ gradient (filled circles), Li⁺ gradient (open circles) and K⁺ gradient (closed triangles), or symmetrical [Na⁺] (open triangles). (B) The same data as in (A), but with the Na⁺ gradient data removed to expand the scale and highlight Li⁺-driven transport.

Figure 3 Na⁺ dependence of ³H-succinate transport activity. Initial rates of ³H-succinate transport as a function of external Na⁺ concentration. A triplicate dataset is averaged (error bars represent s.e.m.) and fit to the Hill equation.

Figure 4 Electrical properties of VcINDY transport. (A) Transport of ³H-succinate into VcINDY-containing liposomes in the presence of an inwardly directed Na⁺ gradient in the presence (open circles, “+Val”) and absence (closed circles, “-Val”) of valinomycin. (B) Modulation of Na⁺-dependent ³H-succinate transport as a function of the voltage across the membrane set with K⁺/valinomycin. Data is from triplicate datasets and the error bars represent s.e.m.

Figure 5 Solute counterflow activity of VcINDY. Solute counterflow activity of VcINDY-containing liposomes in the presence (closed circles, “+Na⁺”) and absence (open squares, “-Na⁺”) of Na⁺. Data is from triplicate datasets and the error bars represent s.e.m.

Figure 6 Substrate interactions with VcINDY. (A) Initial rates of ^3H -succinate transport as a function of external succinate concentration. The data is fit to the Michaelis-Menten equation. (B) Substrate specificity of VcINDY. Initial transport rate of ^3H -succinate into VcINDY-containing proteoliposomes in the presence of an inwardly directed Na^+ gradient at pH 7.5 and 29 potential substrates. Data for each competitor was normalized to the transport rate in the absence of competitor compound. OAA, oxaloacetate; α -KG, α -ketoglutarate; 2,3-DMS, 2,3-dimethylsuccinate; 2,3-DMAS, *Meso*-2,3-dimercaptosuccinate; DMAPS, dimercaptopropane-1-sulfonate; MAS, mercaptosuccinate. All data presented is the average from triplicate datasets and the error bars represent s.e.m. (C) Chemical structures of the four most effective inhibitors; succinate, malate, fumarate and oxaloacetate.

Figure 7 pH dependence of ^3H -succinate transport by VcINDY. The black bars represent the initial accumulation rates of ^3H -succinate into VcINDY-containing liposomes (A, B and C) and empty liposomes (D) under the following conditions; (A and D) fixed internal pH 7.5 and variable external pH, (B) symmetrical variation of pH, and (C) variable internal pH and fixed external pH 7.5. The line graphs represent the theoretical percentage abundance of each protonation state of succinate (gray, deprotonated; red, monoprotonated; green, fully protonated) across the pH range used (percentage abundance was calculated using HySS software (Alderighi et al., 1999)). Below each panel is a schematic representation of the experimental conditions used; the thick black line represents the bilayer, the blue shapes represent VcINDY and the internal and external pHs are noted. The orange and purple arrows indicate the presence of inwardly-directed succinate and Na^+ gradients, respectively. All data presented is the average from triplicate datasets and the error bars represent s.e.m.

Figure 8 Citrate specificity of VcINDY. (A) Theoretical percentage abundance of the protonation states of citrate (block colors; green, deprotonated; yellow, monoprotonated; orange, diprotonated; red, fully protonated) and succinate (lines; blue, deprotonated; purple, monoprotonated; black, fully

protonated) as a function of pH (percentage abundance was calculated using HySS software (Alderighi et al., 1999)). (B) Normalized initial rate of succinate (final concentration of 1 μ M with a radiolabeled to unlabeled ratio of 1:9) transport at pH 7.5, 6.5 and 5.5 in the presence (+) and absence (-) of 1000-fold excess (1 mM) of citrate. (C) Initial rates of ^3H -succinate transport at pH 7.5 (closed circles) and 5.5 (open circles) as a function of citrate concentration. Data is from triplicate datasets and the error bars represent s.e.m.

Figure 9 Determining the orientation of reconstituted VcINDY. (A) Structure of a single VcINDY protomer and its predicted positioning relative to the membrane. The positions of the external cysteine (V343C) and the internal cysteine (A171C, red spheres) are shown as well as the bound citrate (pink spheres) and Na^+ ion (green sphere). (B) Initial transport rates of ^3H -succinate in the presence of an inwardly-directed Na^+ gradient and liposomes containing wildtype VcINDY, cysteine-free VcINDY (cysless), VcINDYA171C, and VcINDYV343C. (C) Coomassie staining (top) and Alexa448 labeling (bottom) of proteoliposomes containing the VcINDY mutants; cysless, VcINDYA171C and VcINDYV343C treated as follows, (1) MM(PEG)12 treatment followed by solubilization and Alexa448-maleimide treatment; (2) solubilization, MM(PEG)12 treatment, Alexa448-maleimide treatment; or (3) solubilization followed by Alexa448-maleimide treatment.

Figure 10 Chloride conductance of VcINDY. Transport of ^3H -succinate in the presence of chloride (“+Cl⁻”, gray lines, data from Figure 2 is redrawn) or methanesulfonate-containing buffers (“-Cl⁻/+MSF”) in the presence (open symbols) and absence (closed symbols) of valinomycin. Data is fit to a single exponential rise to max. Data is from triplicate datasets and the error bars represent s.e.m.

Figure 11 Simple transport scheme of VcINDY. In the outward facing state, VcINDY binds 3 Na^+ ions and single succinate molecule in an unknown order (1). The substrate-bound protein transitions from the outward- to the inward-facing state, presumably via an occluded state (2). Substrate is released in an unknown order into the cytoplasm culminating in an empty, inward-facing state of the protein (3).

The empty protein reverts to the starting position by transitioning from the inward-facing state to the outward facing (4).

Figure 1

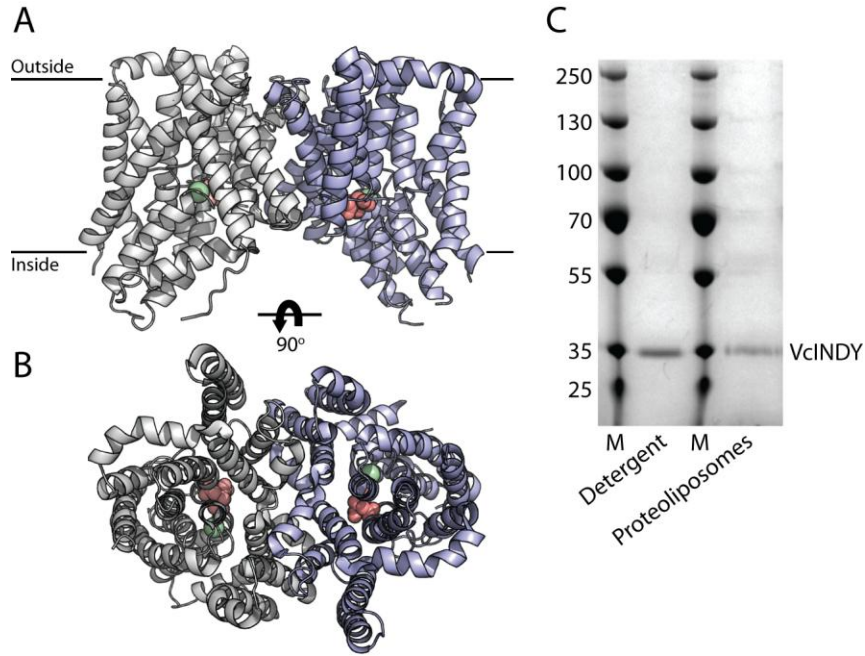


Figure 2

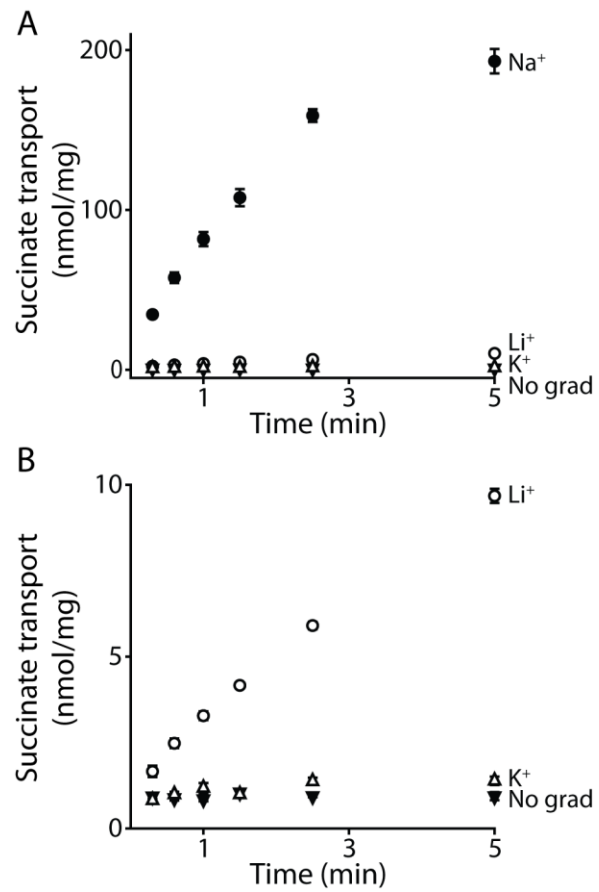


Figure 3

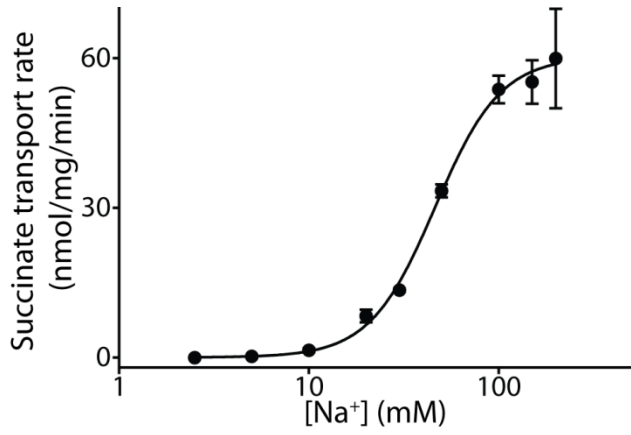


Figure 4

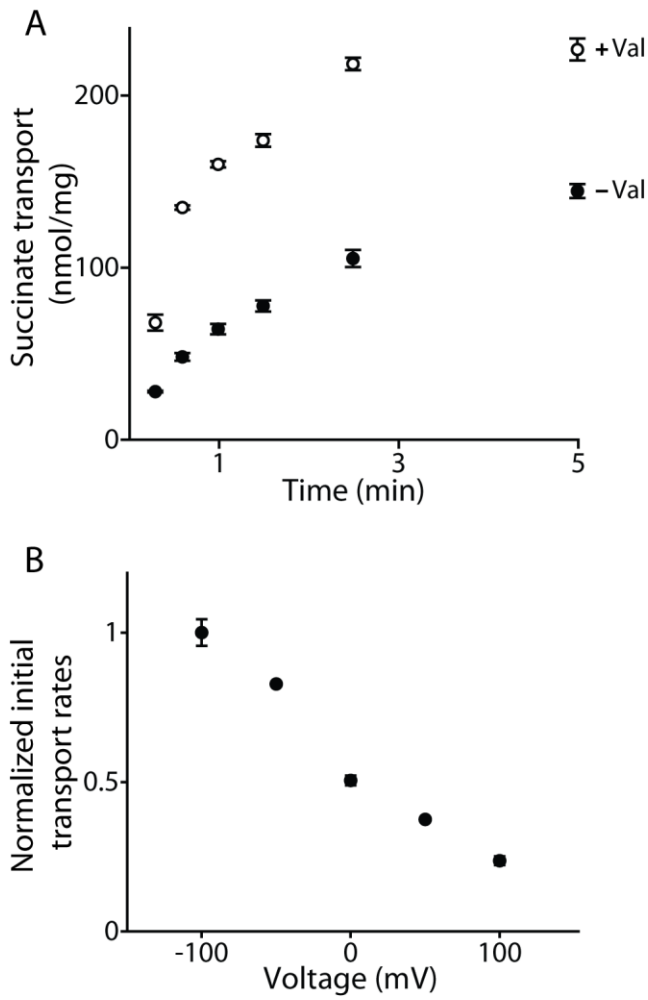


Figure 5

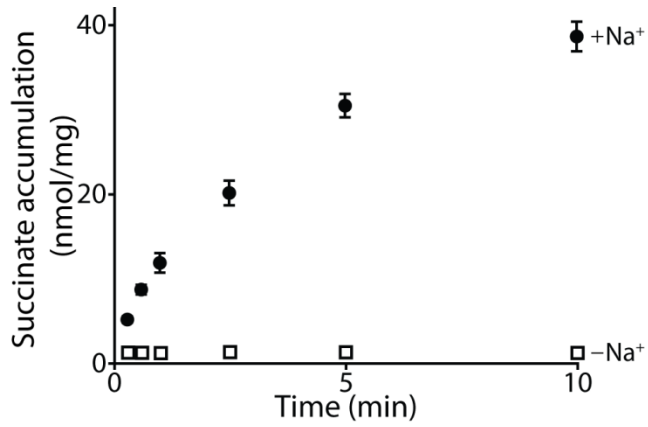


Figure 6

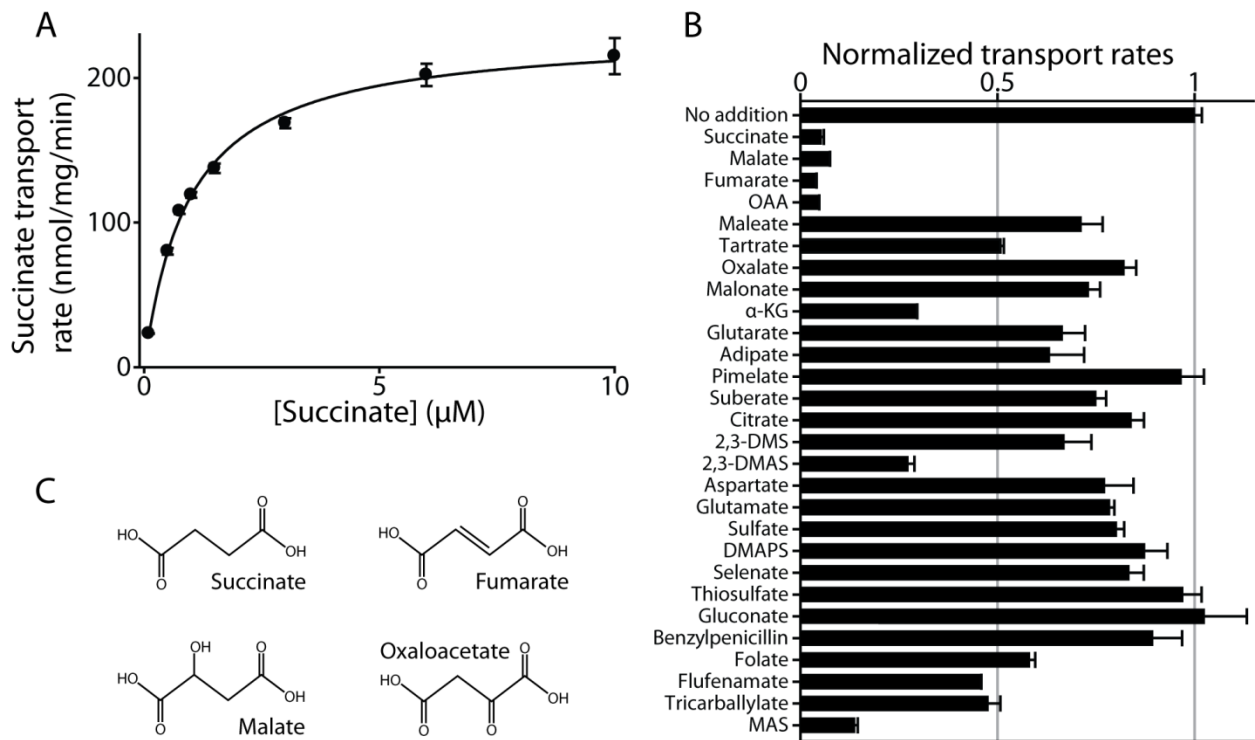


Figure 7

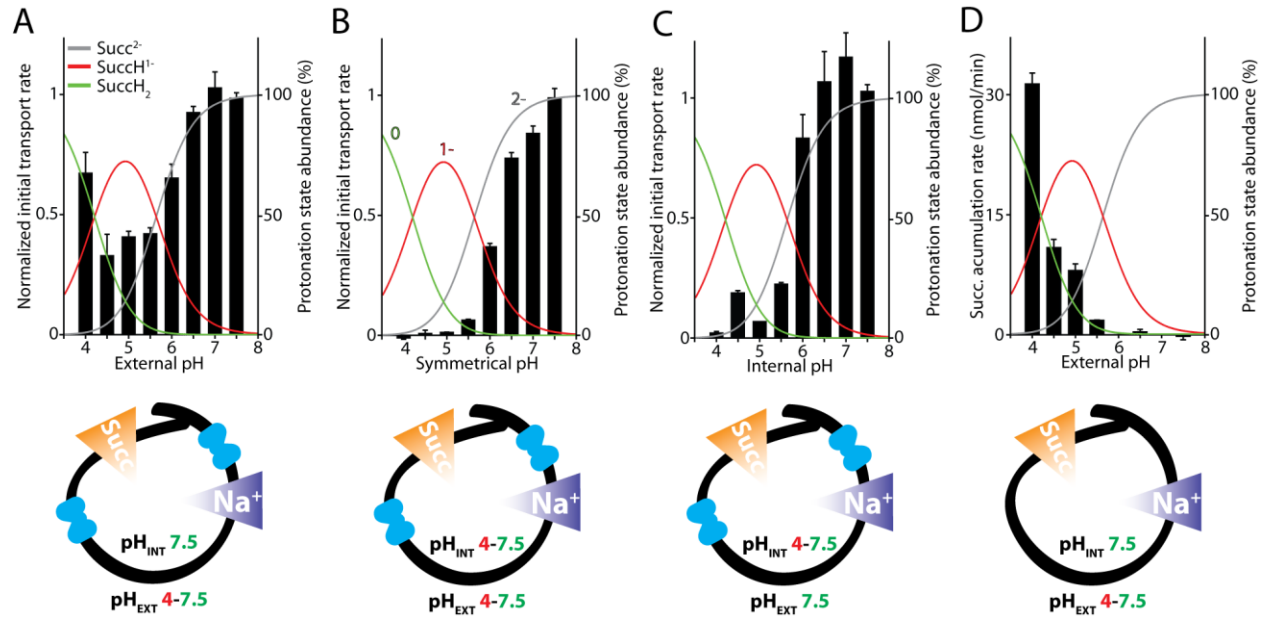


Figure 8

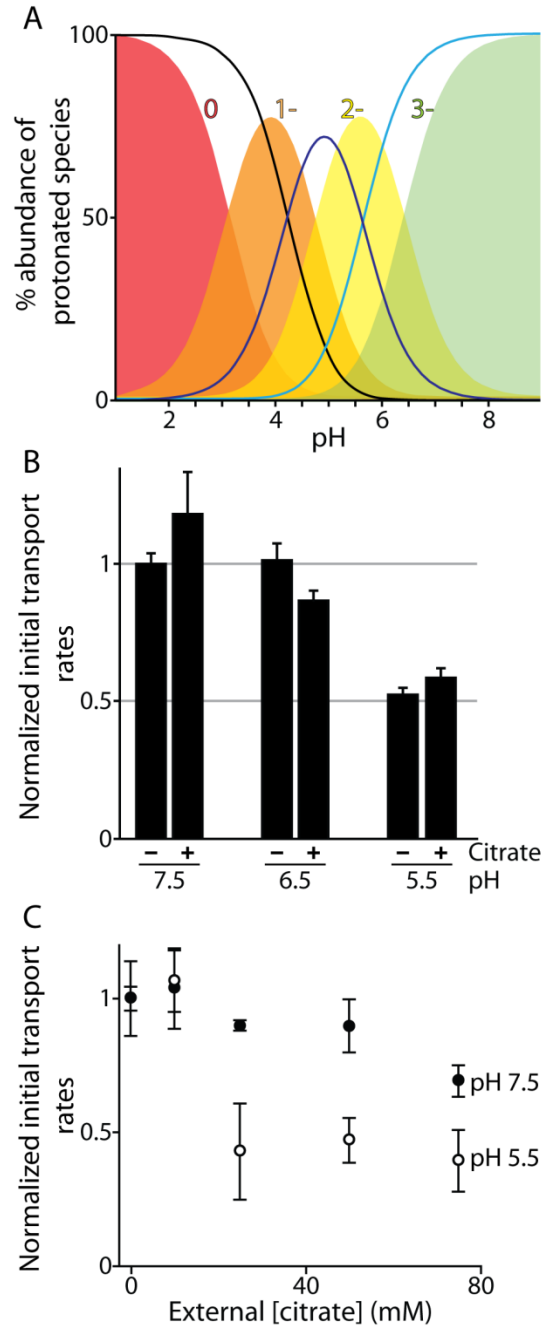


Figure 9

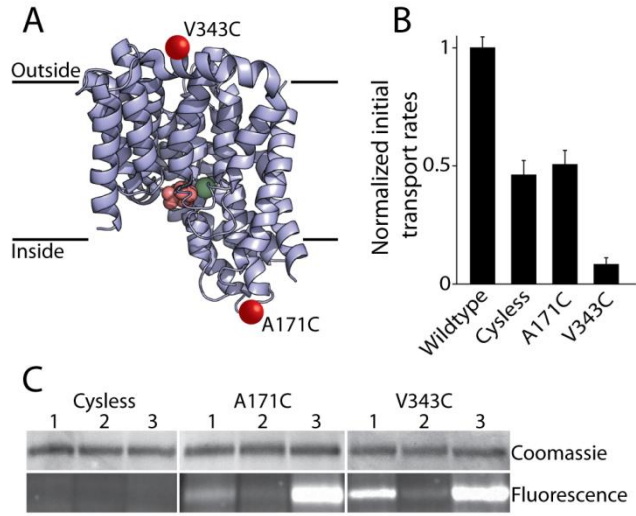


Figure 10

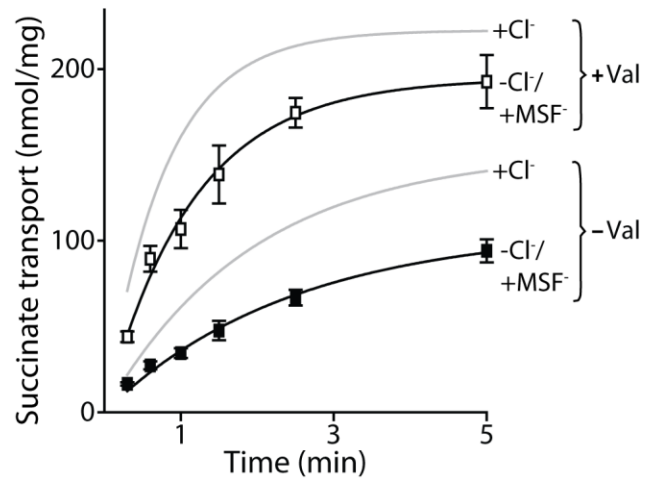


Figure 11

